

# Surface and Interface Structure of Silicon Rich Oxide Films

J. A. Luna-López<sup>1</sup>, M. Aceves-Mijares<sup>1</sup>, J. Rickards<sup>2</sup>, O. Malik<sup>1</sup>, Z. Yu<sup>1</sup>, A. Morales<sup>3</sup>, C. Domínguez<sup>3</sup>, J. Barreto<sup>3</sup>.

<sup>1</sup>Department of Electronic, INAOE, Puebla, Mexico 72000.

<sup>2</sup>Instituto de Física, UNAM, Ap. Postal 20-364, Mexico D.F.

<sup>3</sup>IMB-CNM, Campus UAB. 08193 Bellaterra, España.

Phone +52(222) 247-2011 Fax (222) 247-05-17 E-mail: [jluna@inaoep.mx](mailto:jluna@inaoep.mx), [maceves@iecee.org](mailto:maceves@iecee.org)

**Abstract** — Si nanocrystals are promising materials which can be used for optical sensor, memory devices and future optoelectronics devices. In this work we study the morphology surface and interface of the silicon rich oxide (SRO) films with different nanocrystals (nc-Si) embedded in a thin SiO<sub>2</sub> matrix (Silicon excess). Also the surface roughness after annealing was investigated by means of Atomic Force Microscopy (AFM). AFM images show different morphologies in the surface of the different films. The morphology changes could be associated to the gas flow ratio (Ro) and time of thermal treatment. All images demonstrated grain like structure with size nanometer, which was characterized by height distribution, average roughness, grain and pore mean diameter. X-ray Photoelectron Spectroscopy and Rutherford backscattering spectrometry (RBS) reveals that a small layer formed in the surface of the SRO is SiO<sub>2</sub>, and the composition of the films in the volume varied with respect at the flow ratio, these data have allowed us to correlate the surface and interface structure with the composition of the SRO films.

**Keywords** — Silicon Rich Oxide, AFM, nanocrystals, surface roughness, RBS, XPS.

## I. INTRODUCTION

Thin films of Silicon Rich Oxide (SiO<sub>x</sub>) have been intensively studied because of their technological importance for devices in Silicon based optoelectronics technology. To date, the atomic structures of the films and their physical properties such as the optical and electrical properties have not yet been fully understood. On the other hand, off stoichiometric silicon oxide, also known as silicon rich oxide (SRO), has attracted much research interests in recent years. This material can be considered as a multi-phase material composed of a mixture of stoichiometric silicon oxide (SiO<sub>2</sub>), off stoichiometric oxide (SiO<sub>x</sub>, x<2) and elemental silicon (as nanocrystals). SRO can be prepared by a number of techniques including silicon ion implantation into the thermal dioxide films [1], reactive sputtering [2], co-evaporation [3], low pressure chemical vapor deposition (LPCVD) [4] and plasma enhanced chemical vapor deposition (PECVD) [5]. In all of these techniques, the silicon excess can be controlled by changing the process parameters. Thermal annealing is generally used to modify the structure and to improve the optical and electrical properties of the SRO films, with thermal annealing it is possible to form nanocrystals with size < 10 nm and nanodots with a size ≤ 1 nm. For SRO films prepared by direct deposition of LPCVD, the excess Si may

exist in the oxide matrix in forms of Si clusters, possibly precipitates, or even defective Si-O composites. However, thermal annealing at high temperature (>1000°C) will change it into a two phase material with nc-Si or Si nanodots (crystalline or amorphous) embedded in SiO<sub>2</sub> matrix [6, 7].

In this work, we will present our experimental results on the surface and interface structure of SRO films; the morphology of SRO has been determined by AFM. AFM images show different morphologies in the surface of the different SRO films depending on the gas flow ratio (Ro) and thermal treatment; the annealing caused the grain agglomeration. All images demonstrated grain like structure with nanometer size, which was characterized by height distribution, average roughness and grain and pore average diameter. The composition was obtained by RBS and XPS, these results show a small layer of SiO<sub>2</sub> formed in the surface of the SRO films, and the composition of the films in the volume varied with the flow ratio, Ro.

## II. EXPERIMENT

SRO films were deposited on Silicon (100) substrates. SRO was deposited in an horizontal Low-Pressure Chemical Vapour Deposition (LPCVD) hot wall reactor using SiH<sub>4</sub> (Silane) and N<sub>2</sub>O (nitrous oxide) as reactive gases at 700 °C. The gas flow ratio, Ro = [N<sub>2</sub>O]/[SiH<sub>4</sub>] = 10, 20 and 30, was used to control the amount of excess silicon in the SRO films, and the pressure was varied for each Ro from 1.64-1.94 Torr. After deposition the samples were densified by a thermal annealing at 1000 °C in N<sub>2</sub> during 30 minutes. Some of the densified samples were also thermally annealed at 1100 °C in N<sub>2</sub> during 180 minutes.

The surface morphologies of SRO samples were studied using an easyScan Dynamic Force Microscope (DFM) Nanosurf system version 2.3, operating in a static mode. The topography for each image was measured at a scan size of 4×4 μm<sup>2</sup>. For each sample, several different scans were done and the reproducibility is good. The AFM images were statistically analyzed with the software Scanning Probe Image Processor (SPIP). Average roughness and grain and pores diameter were calculated from AFM images. The oxygen and silicon content of the as deposited SRO films was obtained by RBS of 3.2 MeV α-particles beam of 1 mm diameter, the α-particles were obtained using the 3MV 9SDH-2 Pelletron accelerator and projectiles scattered at 168° were detected with an OXFORD 50-11 surface barrier detector. XPS data were obtained using a PHI ESCA-5500

X-ray photoelectron spectrometer with an Al radiation,  $E = 1486\text{eV}$ . In Table I are listed the samples deposited.

TABLE I  
CLASSIFICATION OF THE SAMPLES OF SRO FILMS

Ro	Without annealing	Densified at 1000 °C in N <sub>2</sub> during 30 minutes	Annealing at 1100 °C in N <sub>2</sub> during 180 minutes
10	BR10	BR10-30	BR10-180
20	BR20	BR20-30	BR20-180
30	BR30	BR30-30	BR30-180

### III. RESULTS

RBS spectra of the as deposited SRO films are shown in Fig. 1. It shows two different spectra corresponding to Ro = 20 and 30, the other two spectra are the respective simulations in order to analyze the RBS spectra and find the oxygen and silicon content in the films, which were done using the SIMRA version 5.02 [8]. In both films, a small layer of SiO<sub>2</sub> was found in the surface. The concentration percentage of silicon and oxygen was determined as 0.43/0.57 and 0.37/0.62 in the bulk SRO for Ro = 20 and Ro = 30, respectively. The layer thickness was determined by RBS to be  $\approx 460$  nm and the superficial layer of SiO<sub>2</sub> is  $\approx 10$  nm for both samples.

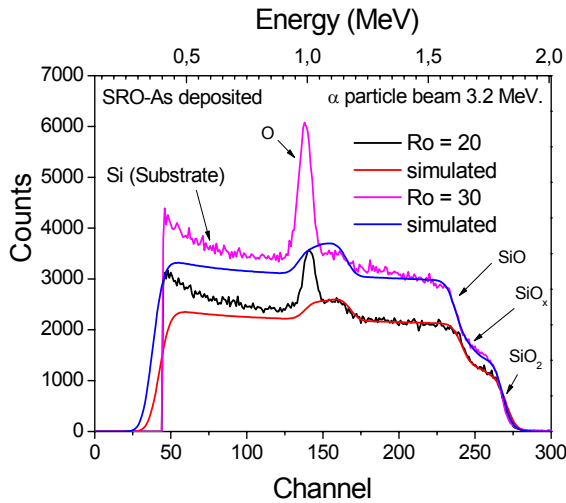


Fig. 1. RBS Spectra for the SRO films. The samples were deposited with a flow ratio Ro = 20 and 30.

The AFM images of SRO films a) as deposited, b) thermally annealed at 1000°C during 30 minutes and c) 1100°C for 180 minutes are presented in Fig. 2. From AFM images, we can see that the surface exhibits different

characteristics depending on the Ro, which influences on the size of the grains (roughness), their form and composition. The average roughness  $\langle Sa \rangle$  measured to Ro = 10, 20 and 30 was 17, 9 and 5, respectively. When the thermal treatment is applied there is a reduction of the height of the roughness and an increased of their area, which is probably due to the agglomeration of the Si nanocrystals [9].

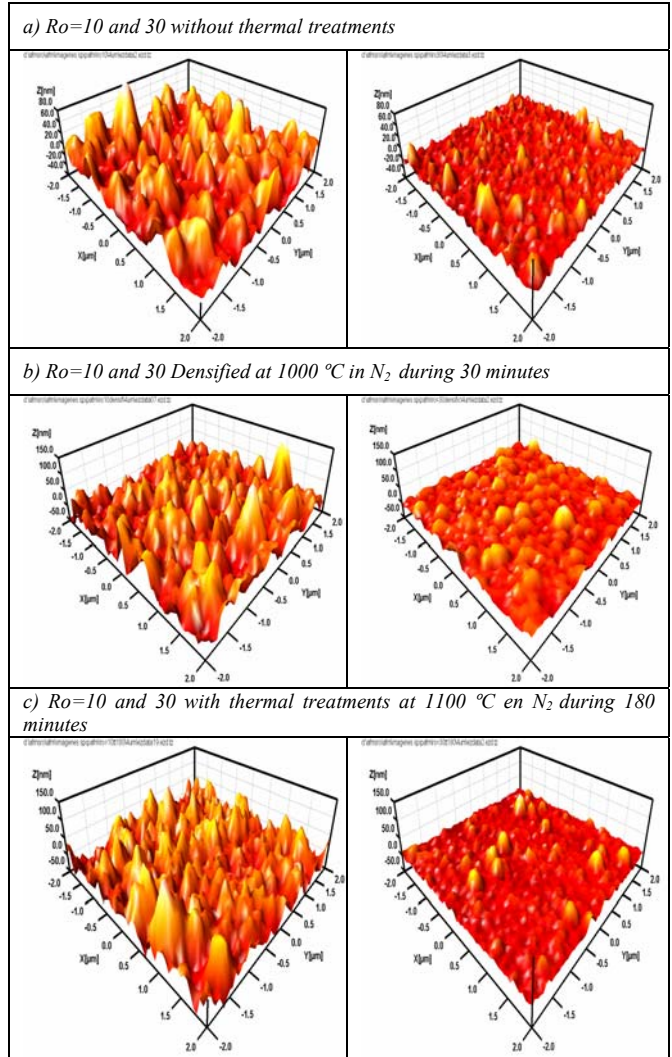


Fig. 2. Comparison AFM images in 3-D to SRO<sub>10</sub> and SRO<sub>30</sub> films without and with thermal annealing, with a size scanner of  $4 \times 4 \mu\text{m}^2$ . The z-scale values in the images are a) 80 nm with step of 20 nm, b) 150 nm with step of 50 nm and c) 150 nm with step of 50 nm, respectively.

Fig. 3 shows XPS experimental spectra of annealed SRO films and the evolution of the Si 2p line in the surface, in the volume and in the SRO/Si interface. Fig. 3 a), b) and c) correspond to Ro = 10, 20 and 30, respectively. The Si 2p region occurs at binding energies from about 98 to 104 eV. The cause of the spectral change is the variation of the composition. In Ro = 10 was showed a peak at about 99.2 eV, in some cases accompanied by a peak at about 103.6

eV, they can be attributed to  $\text{SiO}_2$  and Si, and any variation could be attributed to sub oxidized silicon [10, 11]. The increasing electronegativity of the Si-O bond relative to the Si-Si bond results in a shift to higher binding energy of the core level electrons in the silicon. It is widely accepted that the Si 2p photoelectron peak of  $\text{SiO}_x$  contains five components corresponding to a non oxidized state and four different oxidation states of Si. The four oxidation states as well as the unoxidized state can be modeled as tetrahedral bonding units, in which a central Si atom is bonded to  $(4-n)$  Si atoms and  $n$  oxygen atoms ( $\text{Si-Si}_{4-n}\text{O}_n$ ) with  $n = 0$  to 4. Therefore, for  $\text{SiO}_2$  the 99.2 eV peak is not any more observed, and only 103.6 eV peak corresponding to  $n=4$  is observed.

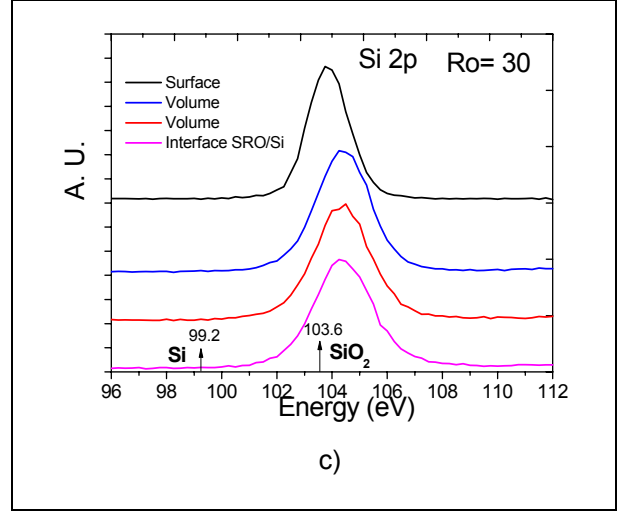
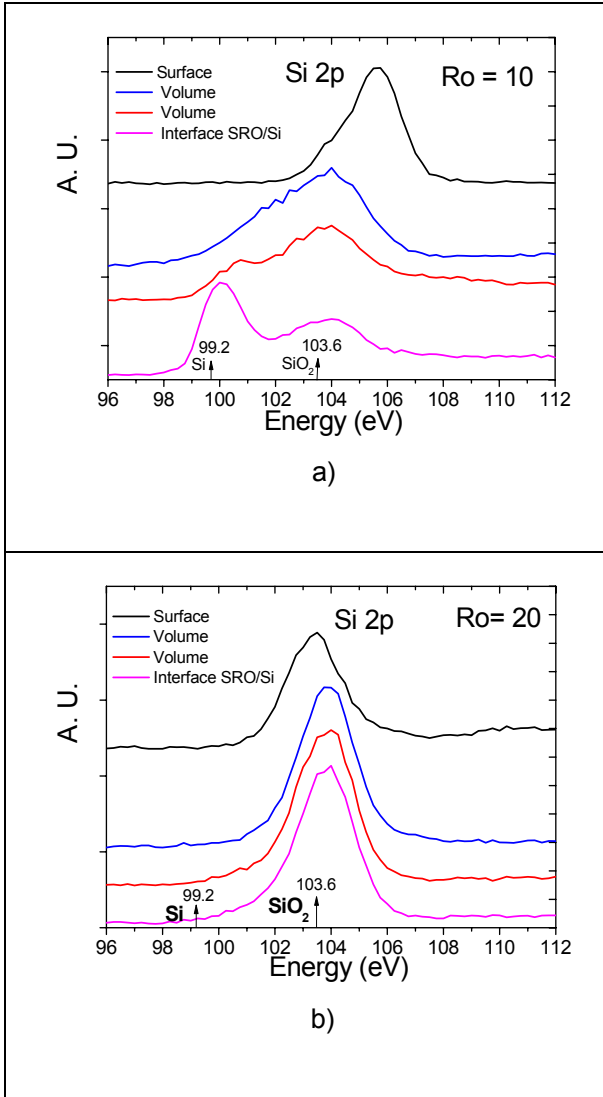


Fig. 3. Si 2p XPS spectra at different position inside the SRO layer, in the surface, volume and interface of the films SRO. Each Si 2p XPS spectra were classify as: a)  $R_o = 10$ , b)  $R_o = 20$  and c)  $R_o = 30$ .

#### IV. ANALYSIS AND DISCUSSION OF RESULTS

The Si concentration of the  $\text{SiO}_x$  ( $x \leq 2$ ) films has been obtained from RBS and XPS measurements. Table II shows a comparison of the results for  $R_o = 20$  and 30.

For  $R_o = 10$  we have different states of oxidation in the films. As can be seen in the top spectrum of Fig. 3 a), in the surface, a peak corresponding to  $\text{SiO}_2$  is observed. In the volume, the peak position shifts towards  $\text{SiO}_2$ , indicative of phase separation and the width increases, then a deconvolution was done and two peaks at 100.5 and 103.6 eV were obtained to  $R_o = 10$ . The peak at 100.5 eV was attributed to elemental Si ( $\text{Si}^0$ ), and the peak at 103.6 eV is  $\text{SiO}_2$  [10, 11]. In the interface, SRO/Si we have two peaks at 100 eV and 103.5 eV, again the first is attributed to elemental Si ( $\text{Si}^0$ ), and the second one at 103.5 eV is  $\text{SiO}_2$ . In other work, to be published, relative big silicon island were observed for SRO films of  $R_o = 10$ . Then this work confirms the TEM observations done in Ref. [12].

For  $R_o = 20$  and 30 the behavior of the curves are similar in the surface, volume and interface, as shown in the Fig. 3 b) and Fig. 3 c), respectively. In the surface a small layer of  $\text{SiO}_2$  is formed, which is represent by peak at 103.4 eV.

In the volume and interface, the peaks are near to 104.4 eV. Also, the elemental silicon peak is weak or vanishes. These two facts indicate the lack of Si nanoclusters in these films. The shifted in the spectra Si 2p is due at the oxidation states of silicon; in this case there isn't the phase separation due to the less silicon excess in the films.

TABLE II  
COMPARISON OF THE COMPOSITION OF  $\text{SiO}_x$  FILMS  
OBTAINED FROM RBS AND XPS MEASUREMENTS

Ro	Without annealing		Annealing at 1100 °C	
	RBS (%)		XPS (%)	
	Si	O	Si	O
20	43	57	38.5	60.8
30	37	62	37.4	62
	Si Silicon	O Oxygen		

The SRO surface morphology was studied with AFM as function of Ro and annealing. The shape of the grain and size in the surface of the SRO films changes due to the flow ratio Ro. In the films without annealing the roughness decrease notably when the silicon excess reduces (17, 9 and 5 nm for Ro = 10, 20 and 30, respectively). With the thermal annealing, in films as deposited, densified at 1000 °C and annealed at 1100 °C the roughness increases in SRO<sub>10</sub> as 17, 22 and 24 nm respectively. But for SRO<sub>20</sub>, the roughness decreases as 10, 7 and 6 nm respectively, and for SRO<sub>30</sub> it also decreases as 8, 7, 5 nm respectively, as shown in the Table III. In figure 4 it is also confirmed that the roughness reduces as Ro increases.

TABLE III  
RESULTS STATISTICS OF AFM OBTAINED TO SRO FILMS

Type Sample	Average Roughness <Sa> (nm)			Grain Diameter <G> (nm)			Pores Diameter <P> (nm)		
	Flow Ratio (Ro)			Flow Ratio (Ro)			Flow Ratio (Ro)		
	10	20	30	10	20	30	10	20	30
As deposited	17	10	8	514	270	206	273	232	132
Densificated at 1000 °C	22	7	7	330	224	331	306	176	158
Annealed at 1100 °C	24	6	5	243	83	167	211	88	129

Fig. 4 shows a statistics analysis of the films' roughness. The height of the peaks is bigger in SRO<sub>10</sub> than SRO<sub>20</sub> and 30, and varied with the thermal annealing. SRO<sub>20</sub> and 30 looks to have the same height, that confirm our idea of the AFM limited measurements, as mentioned. Due to this uncertainty in SRO<sub>20</sub> and 30, the discussion will be centered on the extreme Ro=10 and 30.

As can be seen in Fig. 4 a), the average height of the peaks varies around two times for SRO<sub>10</sub>, but the change for SRO<sub>20</sub> and 30 is almost not noticeable.

From TEM studies in Ref. [9], it has been observed that for silicon excess similar to that of SRO<sub>10</sub>, the thermal annealing at 1100 °C produces agglomerates of Si probably by diffusion [9]. Then, the growth of the peaks in SRO<sub>10</sub> is

related to the growth of the Si agglomerates. Then, for SRO<sub>30</sub> the Si does not agglomerates confirming the RBS and XPS results discussed before. Then, it is likely that SiO<sub>2</sub> compound defects dominate in the SRO<sub>30</sub> rather than Si agglomerates.

In Table III are listed the mean values of roughness <Sa>, grain diameter <G> and pores diameter <P> in function of Ro and thermal treatments. The <Sa>, <G> and <P> are bigger for SRO<sub>10</sub> than for SRO<sub>20</sub> and 30 and varied with the annealing.

In this case, the threshold detection method was used to obtain <G> and <P>. Where, we consider the 1-Dimensional signal. When a threshold is chosen, a binary condition is imposed. Only the part of the segment above the threshold is considered a Grain while the rest is disregarded. Alternatively, the segment parts under the threshold level are the Pores. In Pore mode only pixels under the detection level are considered. The detection and statistical analysis of the Grains/Pores was done using the SPIP Program [13].

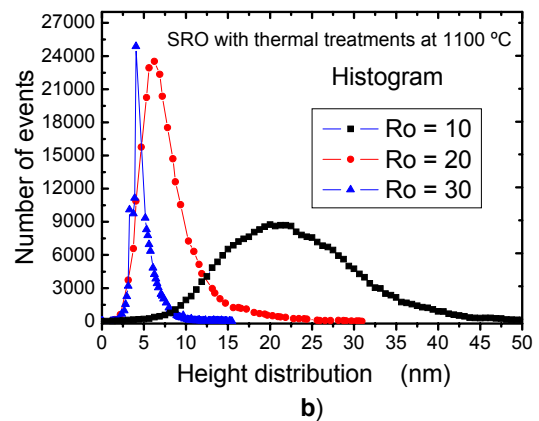
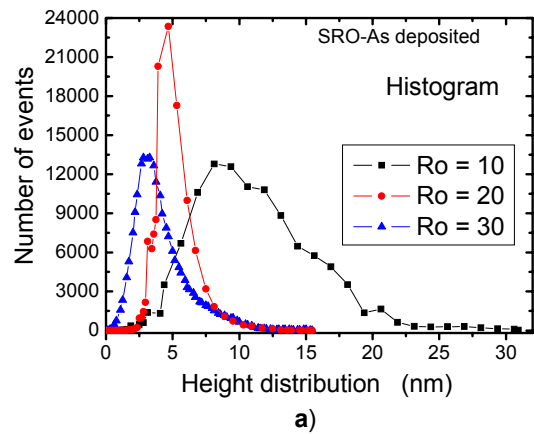


Fig. 4. Peaks' height distribution of the SRO films for a scan area of 4x4  $\mu\text{m}^2$ . Each graphic were classify as: a) SRO films as deposited, b) SRO films with thermal treatments at 1100 °C.

## V. CONCLUSION

In conclusion, RBS, AFM and XPS were all able to measure qualitative differences between SRO films with different silicon excess which varied with the gas flow ratio  $R_o$  and thermal treatments. RBS and XPS allow seeing the differences on the SRO surface, in the bulk and in the interface. The films consisted of three phases: Si-Si,  $SiO_x$  and  $SiO_2$ , depending on the  $R_o$ . AFM was able to analyze the surface morphology of SRO films, where the height, roughness and mean diameter of the grain and pores have a significant change with respect to the flow ratio and different annealing time.

## ACKNOWLEDGMENT

We would like to thank CONACYT and CONCYTEP-FOMIX for providing support to this work. The authors also thank Pablo Alarcón, Mauro Landa, Carlos Zúñiga, Ignacio Juárez and Netzhualecoyotl Carlos for helping in the preparation of the samples and R. Trejo-Luna, K. López, F. Jaimes and A. Heredia by helping in the experiment of RBS.

## REFERENCES

- [1] L. Pavesi, L. Dal Negro, L. Mazzoleni, G. Franzo, and F. Priolo, *Nature*, vol.408, pp440, 2000.
- [2] O. Hanaizumi, K. Ono, and Y. Ogawa, *Appl. Phys. Lett.*, vol.82, pp.538-540, 2003.
- [3] Y. C. Fang, W. Q. Li, L. J. Qi, L. Y. Li, Y. Y. Zhao, Z. J. Zhang, and M. Lu, *Nanotechnology*, vol.15, pp.495-500, 2004.
- [4] D.Dong et al, *J.Electrochem. Soc.*, vol.125, pp.819-823, 1978.
- [5] P. G. Pai, S. S. Chao, and Y. Takagi, *J. Vac. Sci. Technol.*, vol.A4, p.689, 1986.
- [6] J. F. J. Flores, "Study of SRO films and their potential use as radiation sensors", Ph.D. Thesis, INAOE, Tonantzintla, Pue. Mexico, December 2001.
- [7] Fabio Iacona, Glorgia Franzo, and Corrado Spinella, *J. Appl. Phys.*, vol.87, p.1295, 2000.
- [8] Mayer Matej, Software SIMNRA versión 5.02, Max Plank-Institute für Plasmaphysik, D-85748 Garching, Germany, 1997-2004.
- [9] Fabio Iacona, Corrado Borgiono, and Corrado Spinella, *J. Appl. Phys.*, Vol. 95, No. 7, p. 3723-3732, 2004.
- [10] Shinji Hayashi, Shinichi Tanimoto and Keiichi Yamamoto, *J. Appl. Phys.*, Vol. 68, No. 10, p. 5300-5308, 1990.
- [11] L.B. Mag, A.L. Ji, C. Liu, Y. Q. Wang and Z.X. Cao, *J. Vac. Sci. Technol. B*, Vol. 22, No. 6, p. 2654-2657, 2004.
- [12] Zhenrui Yu, Mariano Aceves-Mijares, A. Luna-López, Jinhui Du, and Dongcai Bian, Meeting in Australia, to be published, 2006.
- [13] The Scanning Probe Image Processor (SPIP), image metrology, [www.imagemet.com](http://www.imagemet.com), 2005.